



OPEN

## Solution-derived Ge–Sb–Se–Te phase-change chalcogenide films

Myungkoo Kang<sup>1</sup>✉, Rashi Sharma<sup>2</sup>, Cesar Blanco<sup>2</sup>, Daniel Wiedeman<sup>2</sup>, Quentin Altemose<sup>3</sup>, Patrick E. Lynch<sup>1</sup>, Gil B. J. Sop Tagne<sup>1</sup>, Yifei Zhang<sup>4</sup>, Mikhail Y. Shalaginov<sup>4</sup>, Cosmin-Constantin Popescu<sup>4</sup>, Brandon M. Triplett<sup>5</sup>, Clara Rivero-Baleine<sup>5</sup>, Casey M. Schwarz<sup>3</sup>, Anuradha M. Agarwal<sup>4</sup>, Tian Gu<sup>4</sup>, Juejun Hu<sup>4</sup> & Kathleen A. Richardson<sup>2</sup>

Ge–Sb–Se–Te chalcogenides, namely Se-substituted Ge–Sb–Te, have been developed as an alternative optical phase change material (PCM) with a high figure-of-merit. A need for the integration of such new PCMs onto a variety of photonic platforms has necessitated the development of fabrication processes compatible with diverse material compositions as well as substrates of varying material types, shapes, and sizes. This study explores the application of chemical solution deposition as a method capable of creating conformally coated layers and delves into the resulting modifications in the structural and optical properties of Ge–Sb–Se–Te PCMs. Specifically, we detail the solution-based deposition of Ge–Sb–Se–Te layers and present a comparative analysis with those deposited via thermal evaporation. We also discuss our ongoing endeavor to improve available choice of processing-material combinations and how to realize solution-derived high figure-of-merit optical PCM layers, which will enable a new era for the development of reconfigurable photonic devices.

Dynamic tuning of refractive indices has been explored as a method to better control light propagation. Phase change materials (PCMs) have been identified as one of the key routes to modulation of refractive index ( $n$ ) because they have multiple metastable structures with corresponding electronic states that can be switchable. Switching is realized using a wide variety of energetic stimulations such as temperature, laser or electrical pulses, and mechanical stress<sup>1–12</sup>. The structural transitions lead to changes in their atomic structure and refractive indices. A typical example is a structural transition from amorphous to crystalline states, which induces atomic building blocks to be reconfigured and the medium's electric polarizability to change. Among the wide range of chalcogenide materials used as PCMs, Ge<sub>2</sub>Sb<sub>2</sub>Te<sub>5</sub> has been widely deployed in re-writable media platforms such as DVDs and Blu-ray disks due to its giant contrast in refractive index ( $\Delta n$ ) upon switching as well as its wide operating temperature range<sup>1–3,9–11</sup>. The outstanding optical switching performance of this most industrially adopted PCM has garnered interest in the optics community, and there have been steady efforts to expand the usage of the PCMs toward optical applications, including reconfigurable non-volatile metasurfaces and on-chip photonic modulators<sup>4–8</sup>.

Meanwhile, one of the major bottlenecks in the active deployment of Ge<sub>2</sub>Sb<sub>2</sub>Te<sub>5</sub> as an optical PCM is its broadband optical loss ( $k$ ) in a crystalline state<sup>12</sup>. To explore Ge<sub>2</sub>Sb<sub>2</sub>Te<sub>5</sub>'s compositional variants which do not substantially diminish its desirable key attributes such as large  $\Delta n$  and thermal stability, density functional theory (DFT) modeling of Ge<sub>2</sub>Sb<sub>2</sub>Se<sub>5-x</sub>Te<sub>x</sub> ( $0 \leq x \leq 5$ ) was recently carried out by Zhang et al.<sup>13,14</sup> Specifically, the focus of the computation has been to examine the impact of partial replacement of Te with Se atoms, on the properties of the Ge<sub>2</sub>Sb<sub>2</sub>Se<sub>5-x</sub>Te<sub>x</sub> family. The computation shows that the partial replacement of Te with Se atoms results in an increase in bandgap and reduction in free carrier concentration, thus diminishing  $k$  in the near infrared (IR), while reducing  $\Delta n$ <sup>13,14</sup>. A key conclusion of the computation is that Ge<sub>2</sub>Sb<sub>2</sub>Se<sub>4</sub>Te<sub>1</sub> benefits from lower optical absorption with reduced  $k$  in the near-IR yet still exhibits large  $\Delta n$  via resonant bonding, providing a balanced trade-off between  $k$  and  $\Delta n$ .

Ge<sub>2</sub>Sb<sub>2</sub>Se<sub>4</sub>Te<sub>1</sub>-based PCM alloys have been fabricated as bulk and low-dimensional forms, mainly using standard melt-quench protocols and thermal evaporation (TE), respectively<sup>13–18</sup>. Since the successful introduction and demonstration of Ge<sub>2</sub>Sb<sub>2</sub>Se<sub>4</sub>Te<sub>1</sub> to the optics community using such fabrication techniques, an ability to conformally deposit the PCMs on large-area platforms with nonplanar or complex surface topography

<sup>1</sup>New York State College of Ceramics, Alfred University, Alfred, NY, USA. <sup>2</sup>College of Optics and Photonics, CREOL, University of Central Florida, Orlando, FL, USA. <sup>3</sup>Department of Physics and Astronomy, Ursinus College, Collegeville, PA, USA. <sup>4</sup>Department of Materials Science and Engineering, Massachusetts Institute of Technology, Cambridge, MA, USA. <sup>5</sup>Missile and Fire Control, Lockheed Martin Corporation, Orlando, FL, USA. ✉email: kangm@alfred.edu

has been increasingly desired for the purpose of incorporating them into a wide variety of photonic devices. Chemical solution deposition is a scalable method compatible with substrates of arbitrary shapes and sizes, thus enabling the creation of conformally coated layers<sup>19–22</sup>. It is noteworthy that solution-based binary and ternary telluride PCMs have been recently reported<sup>23</sup>, making the process increasingly adopted in the fabrication of PCMs. While the study is similarly based on the chemical deposition process, there are a couple of key differences. First, our target composition of interest is a direct compositional modification of  $\text{Ge}_2\text{Sb}_2\text{Te}_5$ , where Te has been partially replaced with Se to produce quaternary compounds of Ge–Sb–Se–Te, thus aiming to mitigate the legacy PCM's lingering issue of optical loss while still inducing a large optical contrast upon switching. Second, our study reports the utilization of solution drop-casting to develop a high-throughput scalable deposition and characterization platform. Our manuscript discusses how the process has been employed for Ge–Sb–Se–Te chalcogenide materials, emerging as promising low-loss PCMs, to have desirable phase changes upon switching. Specifically, our study provides an insight on the solution-based process' key parameters and challenges as well as our strategies to mitigate the issues and prepare starting glass layers that can structurally transform into desirable target crystalline phases, assessed by a range of cross-correlating characterization methods. We believe that the progress discussed in our study sets the stage for the further optimization of the solution deposition process specifically tailored for chalcogenide-based PCMs and paves a way toward the assessment of their optical switching performance metrics. We discuss ongoing and future efforts to further improve our processing-material combinations to enable solution-derived  $\text{Ge}_2\text{Sb}_2\text{Se}_{5-x}\text{Te}_x$  layers to be competitively deployable as versatile high performance optical PCMs.

## Results

### Solution-derived $\text{Ge}_2\text{Sb}_2\text{Se}_{5-x}\text{Te}_x$ ( $0.5 \leq x \leq 1.0$ ) from binary ethanethiol-ethylenediamine solvents

The solution-assisted film deposition process begins with the preparation of sources of the target alloy. Bulk alloys of  $\text{Ge}_2\text{Sb}_2\text{Se}_{5-x}\text{Te}_x$  ( $x = 0.5, 0.6, 0.7, \text{ and } 1.0$ ) were made using a traditional melt-quench protocol, commonly employed on chalcogenide glasses<sup>24</sup>. Starting elemental materials were weighed and quantitatively batched into a fused silica ampoule inside a nitrogen-purged glovebox. The ampoule was sealed under vacuum and melted overnight using a rocking furnace at 800 °C to induce spatial homogeneity of the mixture. The melted batch was then air quenched, leading to a bulk alloy. The alloy was taken out of the ampoule and ground into powder which was subsequently filtered through a sieve with an opening diameter of 120 μm to increase their surface to volume ratio and hence solubility within a choice of solvents. The fine powder specimen was dissolved into a homogeneous binary solvent mixture. Polished and plasma cleaned ZnSe substrates were dipped into the solution using a speed controlled robotic arm in an effort to minimize possible variation in film quality associated with inconsistent manual engagement. Finally, the as-coated films undergo soft- and hard-heat treatments at multiple temperatures of 50, 100, and 150 °C to remove residual solvents on a timescale aimed to minimize rapid solvent evolution which might compromise resulting film surface quality (i.e., pinholes and cracks). Figure 1 illustrates the schematic of the process.

Bulk  $\text{Ge}_2\text{Sb}_2\text{Se}_{5-x}\text{Te}_x$  is a multi-phase crystalline material containing micro crystals upon melt-quench process. Since the formation of the crystalline phases is spontaneous, it is challenging to systematically modulate their size, shape, and volume fraction to be consistent under the same repeated melt-quench protocol. It is thus crucial to have structurally consistent source materials so their attributes are present as homogeneous solutions (without phase separation in the liquid state) that can be transferred to coated layers through chemical solution deposition that can serve as a stable base state of PCMs. Such a consistent base state can be achieved by the removal of the crystals, thus conditioning the phase of starting materials to be completely homogeneous. Crystalline phases can be removed during chemical dissolution process where micron-sized powder grains, still containing attributes of their parent alloy, are broken down to molecular or atomic levels and largely lose the periodicity of their crystalline building blocks. Also, it is crucial to dissolve all constituent elements including Ge, Sb, Se, and Te to the same extent to ensure the composition of the parent solution maintains stoichiometry throughout the transition from alloy to solution to that of the final solution-derived films. Therefore, it is important to maximize the solubility of  $\text{Ge}_2\text{Sb}_2\text{Se}_{5-x}\text{Te}_x$  powder, thus necessitating a careful choice of desirable solvent or multi-solvent mixture to yield a stable, well dispersed stoichiometrically homogeneous solution.

As demonstrated previously, Ge and Sb are easily dissolved in a wide variety of amine-based solvents, while Se and Te are notoriously insoluble in most solvents<sup>25,26</sup>. Ethylenediamine (en) dissolves both Se and Te due to its highly nucleophilic nature which fragments them into ion species<sup>21</sup>, but the fragmented elements simultaneously recrystallize back to metallic particles. The competing effect limits the dissolution only to a certain extent. While Se and Te have been also reported to be partially soluble in imidazolium and phosphonium ionic liquids, these solvents possess very low volatilities and are difficult to evaporate upon deposition of films, thus limiting their application for chemical solution deposition<sup>26</sup>. These lingering issues necessitate the usage of a binary or ternary solvent mixture which can exhibit a cooperative effect of three key requirements including (1) the dissolution of all elements, (2) the suppression of recrystallization, and (3) the evaporation of residual solvents. Such a cooperative effect has been recently demonstrated using the addition of ethanethiol (EtSH) to an amine-based solvent<sup>26–28</sup>. Specifically, recent studies indicates that an EtSH-en solvent mixture is reportedly efficient for the dissolution of Se and Te<sup>26–28</sup>. Since Ge and Sb are readily soluble in a wide range of amine-based solvents, EtSH-en was a solvent mixture of choice in our initial study of solution-derived  $\text{Ge}_2\text{Sb}_2\text{Se}_{5-x}\text{Te}_x$ .

A pre-requisite for the usage of EtSH-en as a binary solvent is the ability to form a homogenous mixture, which would enable its cooperative effect to be spatially uniform within a solvent. The mixing ratio of EtSH-en was systematically varied to visually monitor and identify a range of conditions where homogenous solvent mixtures are formed. Figure 2a shows a series of binary solvents with various mixing ratios. Evidently, solvents

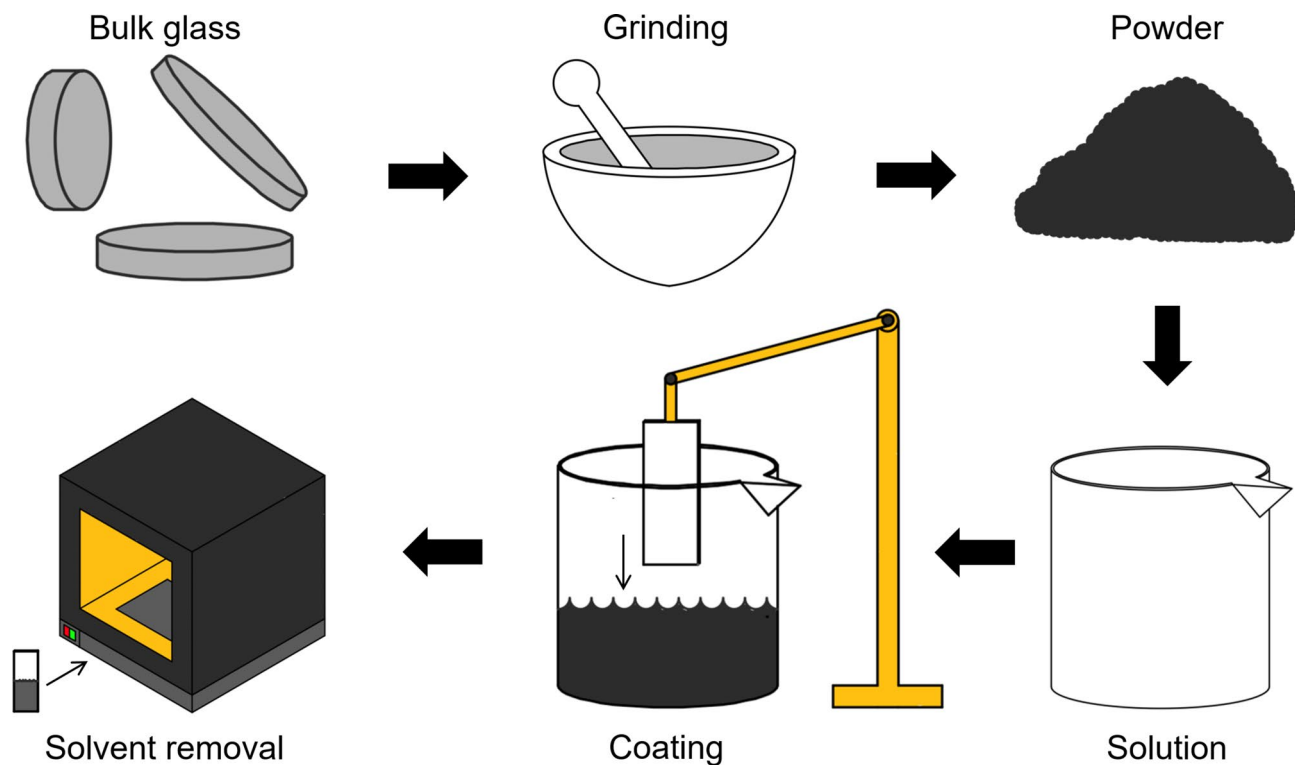


**Figure 1.** A schematic of chemical solution deposition process. Chalcogenide bulk materials with a target composition prepared using a melt-quench process are ground into powder. The powder is then loaded into a custom-designed solvent to form a solution. Subsequently, substrates are dipped into the solution to create films. Finally, residual solvents are removed using thermal bake.

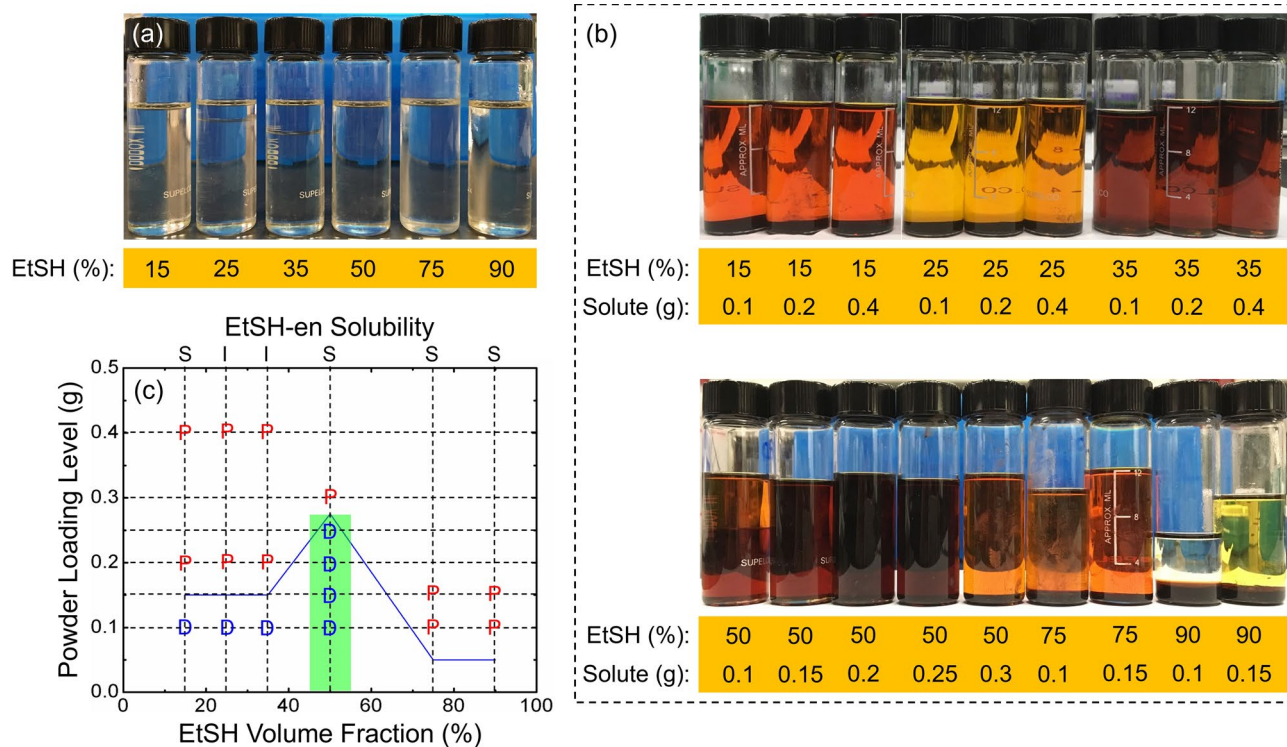


**Figure 2.** (a) Solvent-solvent solubility of binary EtSH-en. (b) Solvent-solute solubility of binary EtSH-en + Ge-Sb-Se-Te powder. (c) A summary map indicating optimal process parameters of solvent composition and solute loading level.

with EtSH's volume fractions of < 25% or > 35% are free of horizontal interfaces indicative of immiscibility and are hence homogenous. Subsequently, the powder solutes were loaded into the same set of solvents with various mixing ratios while their loading level was gradually increased to identify the maximum solubility in each case. Figure 2b shows a series of solutions where over a wide range of loading levels up to 0.25 g as an example, solvents with an EtSH's volume fraction of 50% are still visually transparent while the rest of them indicate their moderate to minimal solubility, leaving undissolved powder on the bottom. Based upon the inter-solvent solubility and solute dissolution tests, a quantitative process window for chemical solution deposition process was constructed, as shown in Fig. 2c. It is important to note that the EtSH's volume fraction of 50% corresponding to the maximum solubility of the powder coincide with the range for the solvent mixture to be homogeneous [green window in Fig. 2c], thus justifying the EtSH's volume fraction of choice in our study.

To further ensure the maximum solubility of powder in the chosen solvent, an additional strategy based on three approaches was employed. First, solutions were aged long enough to maximize the dissolution of the solute. As shown in the inset of Fig. 3a, + 6 h of aging leads to the formation of re-precipitated residues on the top. This is likely due to the gradual evaporation of solvents, indicating a need to stay below the limit. Upon aging, the

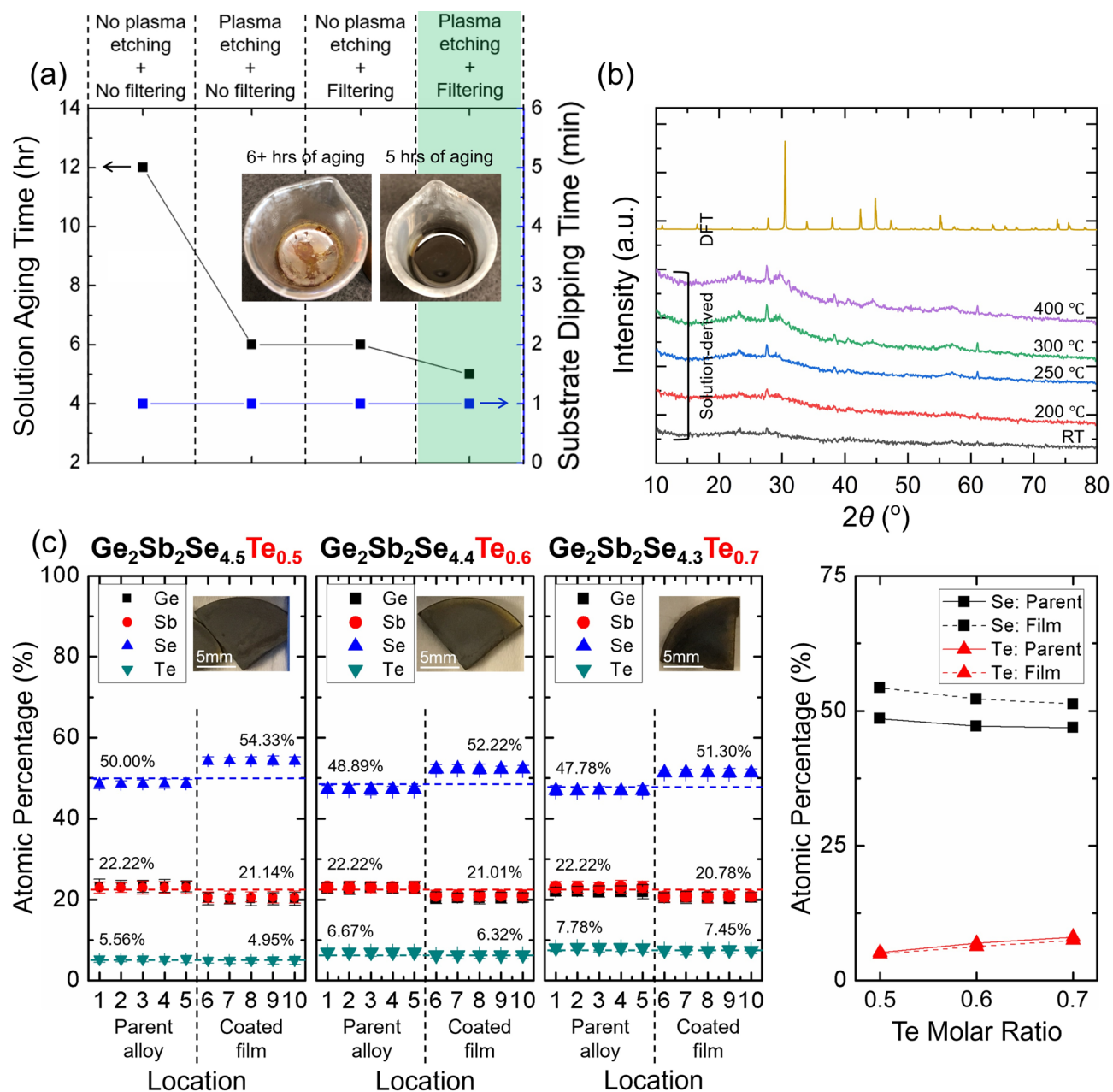


**Figure 3.** (a) A strategy employing a combination of substrate cleaning, solution filtration, and aging processes toward the deposition of high-quality films. (b) In-situ GIXRD data of solution-derived  $\text{Ge}_2\text{Sb}_2\text{Se}_4\text{Te}_1$  films with a DFT-simulated diffraction pattern as a reference. (c) Atomic percentages of constituent elements in  $\text{Ge}_2\text{Sb}_2\text{Se}_{5-x}\text{Te}_x$  ( $x = 0.5, 0.6, \text{ and } 0.7$ ).



solutions underwent a filtration process using a sieve to remove any possibly remaining micron-sized powder. Since contaminants or any surface defects on substrates can also act as sites for the heterogeneous nucleation (i.e., re-precipitation) of dissolved elements, substrates were plasma cleaned. Figure 3 chronicles how the additional strategy has been refined to maximize the solubility of powder.

By employing the solvent mixing ratio and the additional strategy, we expect the nearly complete dissolution and removal of crystals present in the powder solute. To identify the presence of residual crystalline phases, a composition of  $\text{Ge}_2\text{Sb}_2\text{Se}_4\text{Te}_1$  was chosen for a first test. The crystallinity of resulting solution-derived films with the composition was characterized using grazing incidence  $x$ -ray diffraction (GIXRD, see Method for details of instrumental conditions), as shown in Fig. 3b. First, the presence of Te crystals is evident in the as-coated base films, possibly indicating the incomplete dissolution of Te at the sub-micron level. Second, *in-situ* GIXRD data collected up to a maximum temperature of 400 °C, largely mismatched with a density functional theory (DFT)-calculated result<sup>13,14</sup>, indicate that desirable single-phase  $\text{Ge}_2\text{Sb}_2\text{Se}_4\text{Te}_1$  crystals observed in TE-deposited films do not emerge upon thermal treatment. It is likely that Te crystals or minor (likely decomposed) solvent residues disrupt the crystallization energetics of otherwise glassy films, thus suppressing the emergence of the correct  $\text{Ge}_2\text{Sb}_2\text{Se}_4\text{Te}_1$  crystalline phase. Therefore, the amount of Te was correspondingly further adjusted from  $x = 1$  to  $x = 0.7, 0.6$ , and  $0.5$  in  $\text{Ge}_2\text{Sb}_2\text{Se}_{5-x}\text{Te}_x$ , to fully dissolve Te and remove the crystallinity of starting films.

The stoichiometry of as-prepared source materials is carried over to that of solution-derived films under the condition that all constituent elements are fully dissolved in a solution. To identify whether such a compositional transfer was done as intended, the atomic percentages of Ge, Sb, Se, and Te in resulting films were quantified using energy dispersive spectroscopy (EDS), as shown in Fig. 3c. In all cases of  $\text{Ge}_2\text{Sb}_2\text{Se}_{4.3}\text{Te}_{0.7}$ ,  $\text{Ge}_2\text{Sb}_2\text{Se}_{4.4}\text{Te}_{0.6}$ , and  $\text{Ge}_2\text{Sb}_2\text{Se}_{4.5}\text{Te}_{0.5}$  (i.e.,  $x = 0.7, 0.6$ , and  $0.5$  in  $\text{Ge}_2\text{Sb}_2\text{Se}_{5-x}\text{Te}_x$ ), the stoichiometries of their as-prepared parent glass-ceramics and resulting films are consistent. Also, the spatial uniformity of solution-derived films demonstrated in Fig. 3c is consistent with our earlier study where the compositional maps of constituent elements were characterized to be homogeneous over large areas<sup>29</sup>. Figure 4a shows *in-situ* GIXRD data collected from an as-coated based  $\text{Ge}_2\text{Sb}_2\text{Se}_{4.5}\text{Te}_{0.5}$  film where the intensity of peaks associated with Te crystals appears to be suppressed as compared to that from a  $\text{Ge}_2\text{Sb}_2\text{Se}_4\text{Te}_1$  film. A combination of the EDS and *in-situ* GIXRD data confirms the enhanced dissolution and removal of crystals present in the powder solute, setting a stage for a phase change which would involve the generation of a large  $\Delta n$ . Meanwhile, *in-situ* GIXRD data collected at elevated temperatures indicate that three peaks at  $2\theta$  of 31.519, 45.253, and 53.544° begin to appear at a temperature of 400 °C. Their positions and intensity ratio still deviated from those of single-phase  $\text{Ge}_2\text{Sb}_2\text{Se}_4\text{Te}_1$  crystals observed within DFT-simulated and TE-deposited  $\text{Ge}_2\text{Sb}_2\text{Se}_4\text{Te}_1$  films as well as those of other candidate crystalline phases such as  $\text{Sb}_2\text{Te}_3$  (JCPDS #15-0874) and  $\text{Sb}_2\text{Se}_3$  (JCPDS #15-0861)<sup>30,31</sup>.

A rationale behind the partial replacement of Te with Se in  $\text{Ge}_2\text{Sb}_2\text{Te}_5$  is based on an ability to mitigate  $k$  while still being able to generate a reasonable  $\Delta n$  upon switching. The performance of optical PCM is quantified using a figure of merit ( $\Delta n/k$ ) where Te is largely responsible for both  $\Delta n$  and  $k$ . In addition to realizing a large  $\Delta n$  through the generation of desirable high- $n$  crystalline phases, it is important to consider  $k$  in order to assess  $\Delta n/k$  of our solution-derived films. Figure 4b shows IR transmission spectra (Fresnel reflection not counted) collected from as-coated and heat-treated films. Both of the films with base and switched states exhibit broadband transparency over mid- to long-wave IR spectral range. Meanwhile, heat treatment induces a noticeable decrease in the short-wave IR transparency of the film, likely attributed to increased Fresnel reflection from the increased refractive index, reduction in bandgap, and emergence of free carrier absorption that occur due to the crystallization process<sup>32</sup>.

Beyond blanket thermal treatment, the ability to locally convert PCMs in a spatially defined manner is one of key pre-requisites to their applicability to be incorporated into devices. To assess the local switching of solution-derived films, a series of surface patterns were created using sub-ablation near-bandgap femtosecond direct laser writing with a center wavelength of 801 nm with varying power densities, as shown in Fig. 4c. The feature written in a serpentine pattern becomes visually brighter with increasing laser power density, consistent with the fact that an increase in laser power density is expected to induce a higher  $n$ , thus leading to a higher Fresnel reflection at the surface. Figure 4d shows Raman spectra collected from as-deposited and laser-written areas with a comparison made to those from TE-deposited films. While the solution-derived and TE-deposited films share common spectral signatures at wavenumbers of 115, 155, and 188  $\text{cm}^{-1}$ , close to 120  $\text{cm}^{-1}$  ( $\text{GeSe}_6$  octahedra), 157  $\text{cm}^{-1}$  ( $\text{GeSe}_4$  tetrahedra), and 192  $\text{cm}^{-1}$  ( $\text{SbSe}_6$  octahedra) reported to be observed in magnetron plasma sputtered  $\text{Ge}_2\text{Sb}_2\text{Se}_4\text{Te}_1$  films<sup>33</sup>, a large portion of their spectra mismatch. Also, the development of the spectral signature at a wavenumber of 115  $\text{cm}^{-1}$  for TE-deposited films, associated with the emergence of single-phase  $\text{Ge}_2\text{Sb}_2\text{Se}_4\text{Te}_1$  crystals, is shown for solution-derived films but to a much lesser extent. It noteworthy that the Raman features observed for solution-derived films are likewise deviated from those reported for other candidate crystalline phases such as  $\text{Sb}_2\text{Te}_3$  and  $\text{Sb}_2\text{Se}_3$ <sup>34–37</sup>. The inconsistency in their switching behaviors as well as their anomalies in GIXRD and FT-IR data necessitates us to understand the possible role of reduced but extant Te and minor decomposed solvent residues on the switching behavior of the solution-derived films and revisit our strategy to dissolve constituent elements to completion.

To elucidate the behavior of the binary EtSH-en solvent, its spectral signatures were monitored as a function of time, using attenuated total reflectance-Fourier transform infrared (ATR-FTIR) spectroscopy. Figure 5a shows optical transparency of EtSH, en, and a binary EtSH solvent as well as a solution consisting of the binary solvent and  $\text{Ge}_2\text{Sb}_2\text{Se}_{4.5}\text{Te}_{0.5}$  powder. Two absorption bands at  $\lambda = 7.4$  and  $7.9 \mu\text{m}$ , associated with en and EtSH, respectively, are individually traceable in the binary solvent mixture and the solution. The time-dependent evolution of the two spectral features in the solvent and the solution was then monitored as shown in Fig. 5b and c, where the feature at  $\lambda = 7.9 \mu\text{m}$  (EtSH) is observed to change to an extent much greater than its counterpart. Figure 5d shows the time-dependent intensity ratios of EtSH's spectral absorption band to that of en in the solvent and the solution. In both cases, the ratio significantly decreases as a function of time, strongly indicating

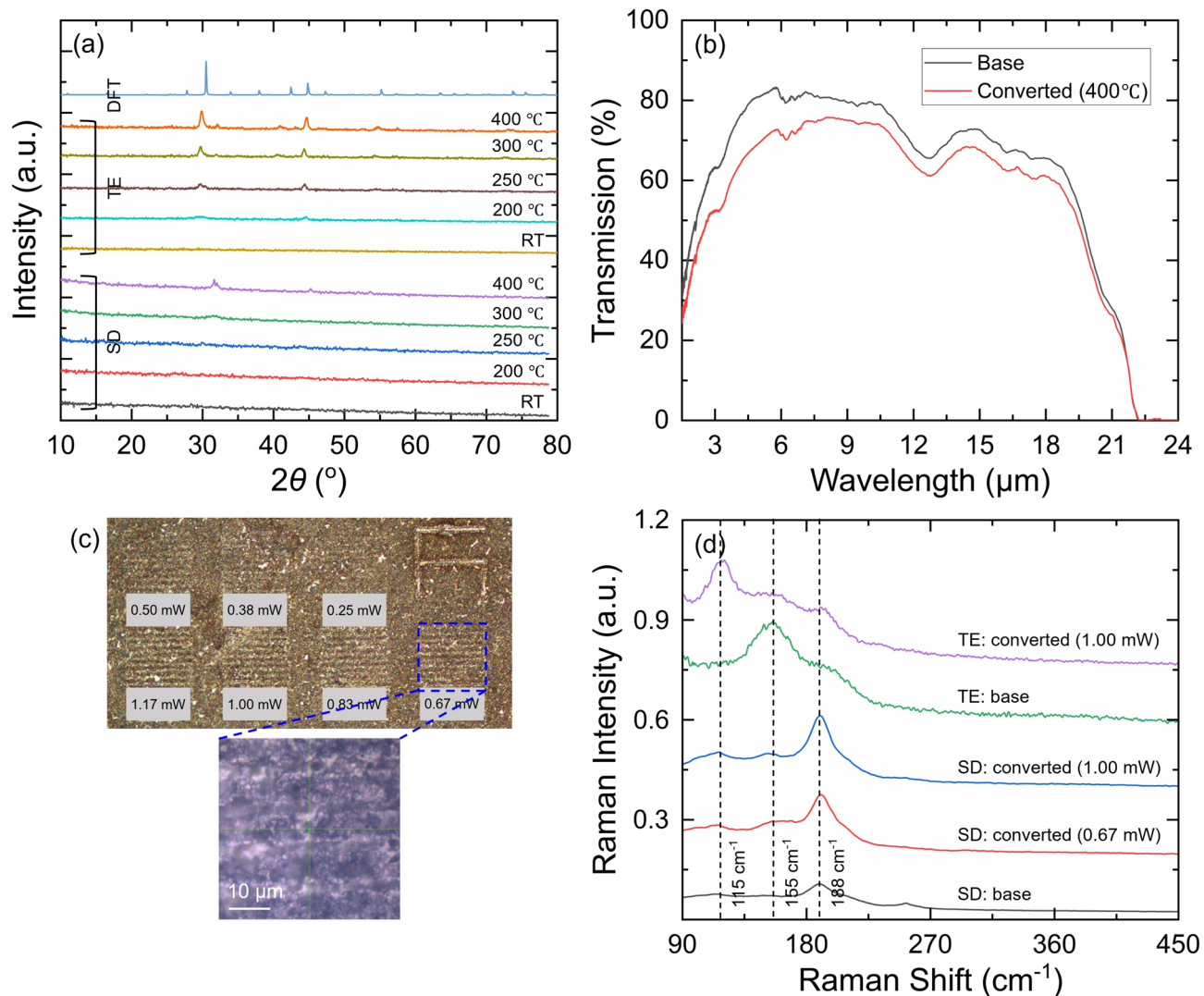


**Figure 4.** (a) In-situ GIXRD data of solution-derived  $\text{Ge}_2\text{Sb}_2\text{Se}_{4.5}\text{Te}_{0.5}$  films with TE-deposited  $\text{Ge}_2\text{Sb}_2\text{Se}_4\text{Te}_1$  films and a DFT-simulated diffraction pattern as references. (b) Transmission of solution-derived  $\text{Ge}_2\text{Sb}_2\text{Se}_{4.5}\text{Te}_{0.5}$  films prior to and post thermal switching. (c) A series of surface patterns were created using sub-ablation near-bandgap direct laser writing with varying power densities. (d) Raman spectra collected from as-deposited and laser-written areas with a comparison made to those from TE-deposited films.

the preferential evaporation of EtSH. While the binary EtSH-en solvent was demonstrated to be efficient for the dissolution of four constituent elements, its function is temporally limited, necessitating us to search for a better solvent of choice.

#### Solution-derived $\text{Ge}_2\text{Sb}_2\text{Se}_{5-x}\text{Te}_x$ ( $x=1.0$ ) from binary 1,2-ethanedithiol-ethylenediamine solvents

Exploring innovative and environmentally safer solvent chemistries has been driven by the desire to efficiently deposit  $\text{Ge}_2\text{Sb}_2\text{Se}_{5-x}\text{Te}_x$  ( $x=1.0$ ) films. In this section, we discuss the deposition of  $\text{Ge}_2\text{Sb}_2\text{Se}_4\text{Te}_1$  through drop-casting, employing a promising cost-effective methodology for realizing specific spatial regions of films, such as on a planar platform. The method utilizes a novel alkahest solution composed of ethylenediamine (en) and 1,2-ethanedithiol (Edtsh)<sup>38</sup>. This binary solvent mixture demonstrates an exceptional ability to dissolve bulk chalcogenides at room temperature. Notably, tellurium, known for its low solubility in most solvents, readily dissolves in the en:Edtsh binary solvent mixture at room temperature<sup>26</sup>. The outcomes of the study spurred our team to utilize the binary alkahest solvent mixture of en:Edtsh for dissolving  $\text{Ge}_2\text{Sb}_2\text{Se}_4\text{Te}_1$ . To maintain the integrity of the solvent and prevent oxidation of both the solvent and the deposited film, precursor solutions were meticulously prepared within a nitrogen-filled glove box (with  $\text{H}_2\text{O}$  and  $\text{O}_2$  levels below 0.1 ppm). A volume-to-volume ratio of 1:10 for the binary solvent mixture exhibited exceptional solubility for  $\text{Ge}_2\text{Sb}_2\text{Se}_4\text{Te}_1$ . To delve deeper into the investigation, various loading levels of  $\text{Ge}_2\text{Sb}_2\text{Se}_4\text{Te}_1$  were introduced into the volume-to-volume ratio of for en:Edtsh. In Fig. 6a, a photograph depicts  $\text{Ge}_2\text{Sb}_2\text{Se}_4\text{Te}_1$  with loading levels from 0.5 to 5.8 weight percentages (wt%) dissolved in en:Edtsh with a volume-to-volume ratio of 10:1 at room temperature (25 °C)

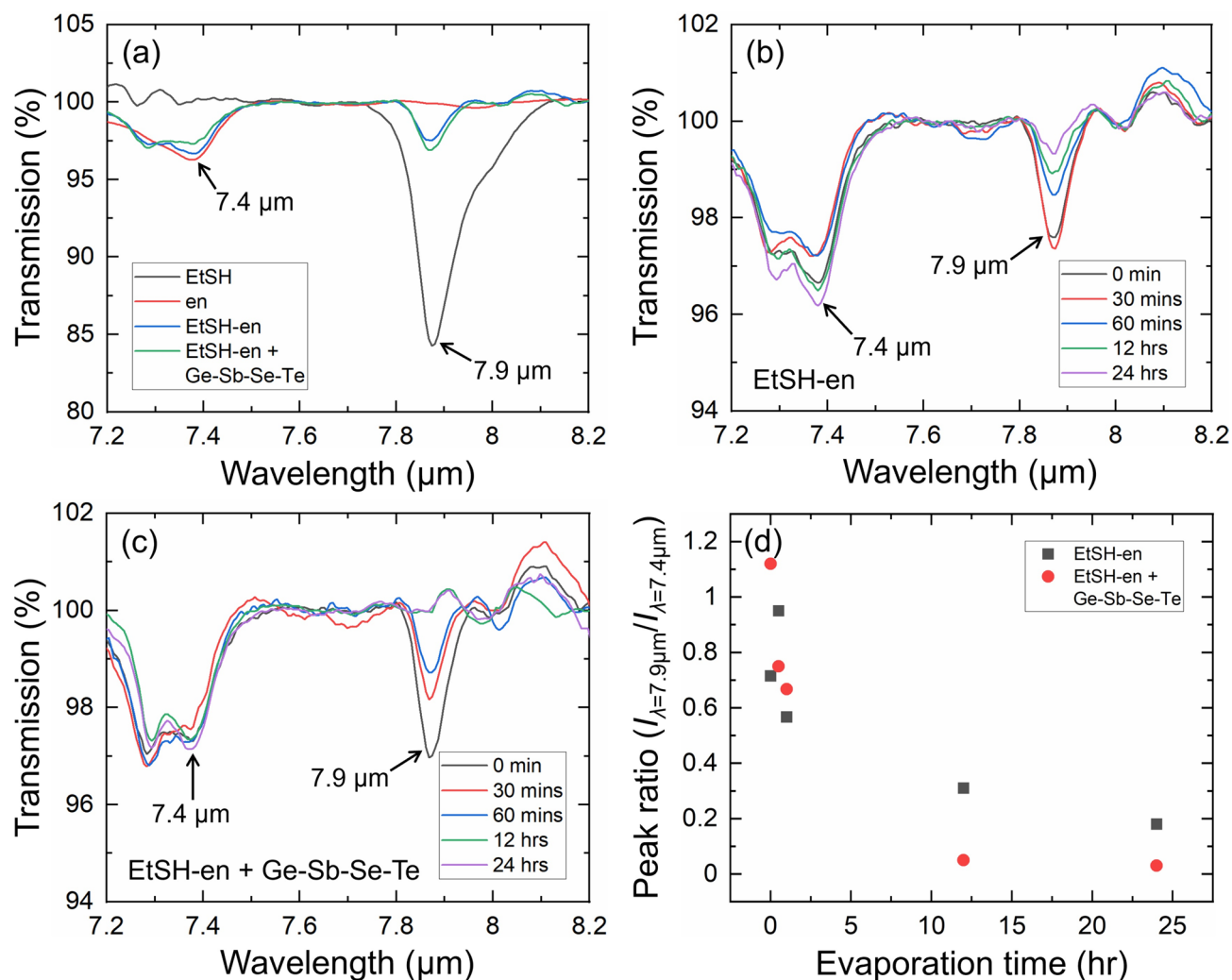


**Figure 5.** (a) Transmission spectra of EtSH, en, and a binary EtSH-en solvent as well as a solution consisting of the binary solvent and Ge-Sb-Se-Te powder. (b) The time-dependent transmission spectra of the binary solvent. (c) The time-dependent transmission spectra of the solution. (d) The time-dependent ratio of the characteristic spectral signature at a wavelength of 7.9  $\mu\text{m}$  (EtSH) to that at a wavelength of 7.4  $\mu\text{m}$  (en).

over a 24-h period. All solutions displayed a dark brown color, and those with loading levels below 2.5 wt% were optically transparent, devoid of visible scattering, as illustrated in Fig. 6b.

The transmission spectra of the individual solvents of en and Edtsh were contrasted with the en:Edtsh mixture with a volume-to-volume ratio of 10:1. In Fig. 7a, two distinct peaks emerged at  $\lambda = 7.9 \mu\text{m}$  and  $8.4 \mu\text{m}$ . The peak at  $\lambda = 7.9 \mu\text{m}$  indicates the presence of Edtsh, while the peak at  $\lambda = 8.4 \mu\text{m}$  signals the presence of en in the solution. Subsequently, the en:Edtsh mixture with a volume-to-volume ratio of 10:1 was kept at room temperature, and the disappearance of the peaks at  $\lambda = 7.9 \mu\text{m}$  and  $8.4 \mu\text{m}$  was observed over time, as depicted in Fig. 7b. Upon standing at room temperature, the peak intensity at  $\lambda = 7.9 \mu\text{m}$  decreased by approximately 1.1%, while no change in the peak intensity at  $\lambda = 8.4 \mu\text{m}$  was noted (though alterations in peak shapes were observed). This lack of change in the peak intensity at  $\lambda = 8.4 \mu\text{m}$  suggests a preferential evaporation of Edtsh from the en:Edtsh solution mixture. For the determination of the optimal bake protocol (time and temperature) required for complete solvent evaporation,  $\text{Ge}_2\text{Sb}_2\text{Se}_4\text{Te}_1$  dissolved in en:Edtsh solvent was drop-casted onto a cleaned ZnSe substrate. The transmission spectra of the solvent evaporation are presented in Fig. 7c. Initially, the film underwent a soft bake at  $40^\circ\text{C}$ , followed by a hard bake up to  $150^\circ\text{C}$ . It is noteworthy that the shape of the peaks at  $\lambda = 7.9 \mu\text{m}$  and  $8.4 \mu\text{m}$  exhibited variations after the addition of  $\text{Ge}_2\text{Sb}_2\text{Se}_4\text{Te}_1$  alloy to the solvent mixture. The solvent mixture evaporation was observable up to  $210^\circ\text{C}$ , but complete confirmation via FT-IR spectroscopy was hindered due to film formation causing high scattering. Subsequently, the ZnSe substrate was heated at  $210^\circ\text{C}$  for 3 h, and solvent evaporation was observed through EDS, as illustrated in Fig. 7d. The absence of S and N in the EDS spectra of the film verified the significant reduction of the solvent mixture. However, the presence of C in the film indicated the existence of by-products, potentially explaining the atomic % difference between the film and the bulk  $\text{Ge}_2\text{Sb}_2\text{Se}_4\text{Te}_1$  alloy.

The initial investigation into solvent behavior aimed to establish the solubility limit of the  $\text{Ge}_2\text{Sb}_2\text{Se}_4\text{Te}_1$  alloy in the en:Edtsh binary solvent mixture and develop an evaporation protocol ensuring complete solvent removal with minimal impurities, specifically a few at% of C. For this, a  $\text{Ge}_2\text{Sb}_2\text{Se}_4\text{Te}_1$  solution with a loading level of 1.25

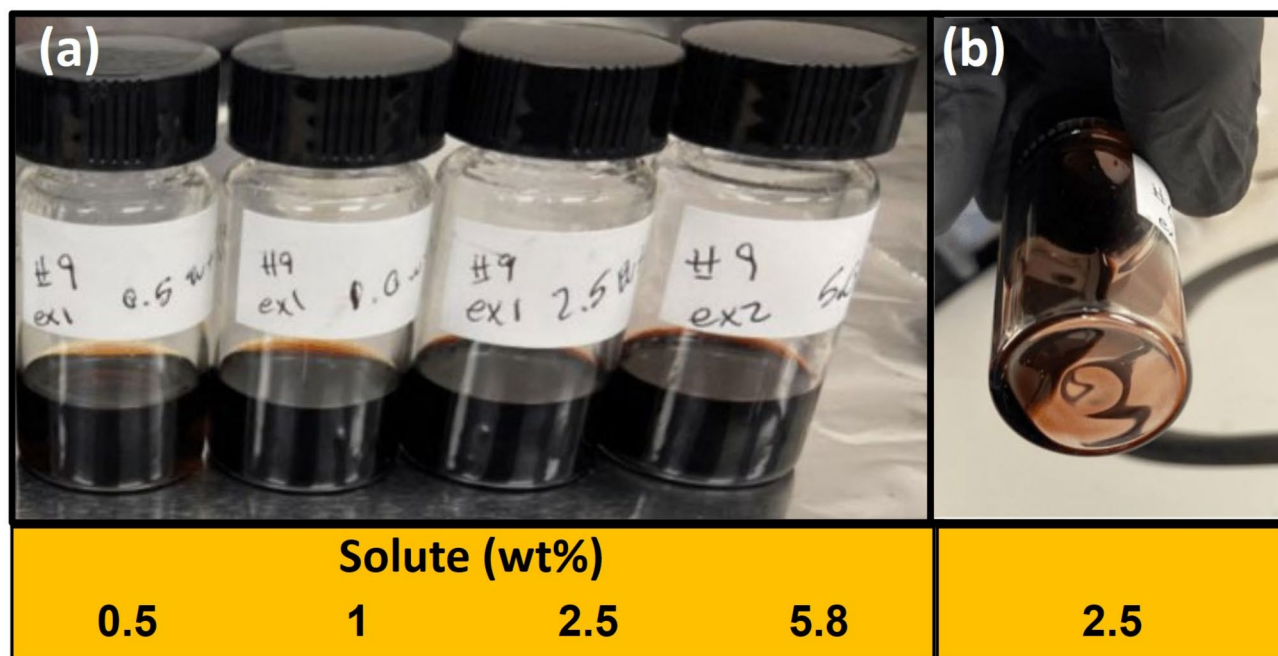


**Figure 6.** (a)  $\text{Ge}_2\text{Sb}_2\text{Se}_4\text{Te}_1$  dissolved in binary en:Edtsh solvent with a volume to volume ratio of 10:1. (b) Complete dissolution of  $\text{Ge}_2\text{Sb}_2\text{Se}_4\text{Te}_1$  powder in solvent with a loading level of 2.5 wt%.

wt% was drop-casted onto a  $\text{TiO}_2$ -coated Si substrate. The film underwent a controlled heating process at a ramp rate of  $2^\circ\text{C}/\text{min}$  up to  $350^\circ\text{C}$ , dwelling for 20 min, and gradually cooled down to room temperature. Figure 8a presents the initial characterization of the film through GIXRD, comparing the XRD of the drop-casted film with the bulk  $\text{Ge}_2\text{Sb}_2\text{Se}_4\text{Te}_1$  alloy. The presence and absence of certain crystallization peaks confirms that the film undergoes crystallization during solvent evaporation. Predominant peaks from the bulk  $\text{Ge}_2\text{Sb}_2\text{Se}_4\text{Te}_1$  alloy at  $2\theta = 29.103^\circ$ ,  $30.039^\circ$ ,  $40.433^\circ$ , and  $43.675^\circ$  were observed in its solution-derived film. Additionally, some  $\text{Sb}_2\text{Se}_3$  crystallization peaks at  $2\theta = 17.525^\circ$  and  $39.625^\circ$  were present, indicating a complex crystallization pattern. However, the film displayed the absence of Te peaks, suggesting the avoidance of early Te precipitation. In Fig. 8b, the surface morphology of the  $\text{Ge}_2\text{Sb}_2\text{Se}_4\text{Te}_1$  film is depicted using SEM, revealing particles with an average length ranging from  $2\ \mu\text{m}$  to  $200\ \text{nm}$ . The drop-casted Ge–Sb–Se–Te film depicted here serves as an example of the preliminary efforts in developing a solution-based deposition method for a quaternary Ge–Sb–Se–Te PCMs. The use of co-solvents, specifically en and Edtsh, has facilitated the complete solubility of Ge–Sb–Se–Te. XRD analysis of the drop-casted film not only confirms the presence of the  $\text{Ge}_2\text{Sb}_2\text{Se}_4\text{Te}_1$  alloy but also indicates the absence of Te peaks, suggesting the stability of this solvent blend. Additionally, adjustments in solubility and deposition temperatures contribute to minimizing particle size (polytelluride chains) within the film, thereby controlling film thickness<sup>23,39</sup>.

### Conclusion and outlook

Chalcogenide  $\text{Ge}_2\text{Sb}_2\text{Se}_{5-x}\text{Te}_x$  films ( $0.5 \leq x \leq 1.0$ ) were fabricated using the chemical solution deposition process as an alternative PCM to partially substitute Te with Se in optically lossy  $\text{Ge}_2\text{Sb}_2\text{Te}_5$ , while greatly increasing design flexibility toward the realization of conformal reconfigurable media. This synergistic outcome is enabled by the combination of a new composition chosen to realize a high figure-of-merit and the solution process compatible with diverse compositions as well as substrate geometries. We systematically refined the chemical solution deposition process to further improve the dissolution of parent glass–ceramic powder. While the chemical solution deposition process has been considered advantageous over standard methods using e-beam evaporation and sputtering techniques as a route toward the realization of scalability and conformal coating, it has challenges. For example, just as each source material's evaporation or sputtering rate needs to be precisely tuned for the standard methods, our study indicates that chemical solution deposition process necessitates a delicate maxing ratio of constituent solvents. It is also crucial to remove residual solvents to avoid any potential undesirable impact on the development of crystalline phases upon switching. Further insight into potential for the improvement of solution-derived films and their advantages over traditional PCMs would be revealed by the rigorous assessment of their figure-of-merit in a wide spectral range. Our team is currently focusing on the solution-based deposition of  $\text{Ge}_2\text{Sb}_2\text{Se}_4\text{Te}_1$  and  $\text{Sb}_2\text{Se}_3$  films as well as the characterization of their optical functionality as phase change memory materials in prototype *in-situ* phase change devices<sup>40</sup>. Both fundamental and practical natures of the novel deposition approach studied here may not only shed light on the lingering



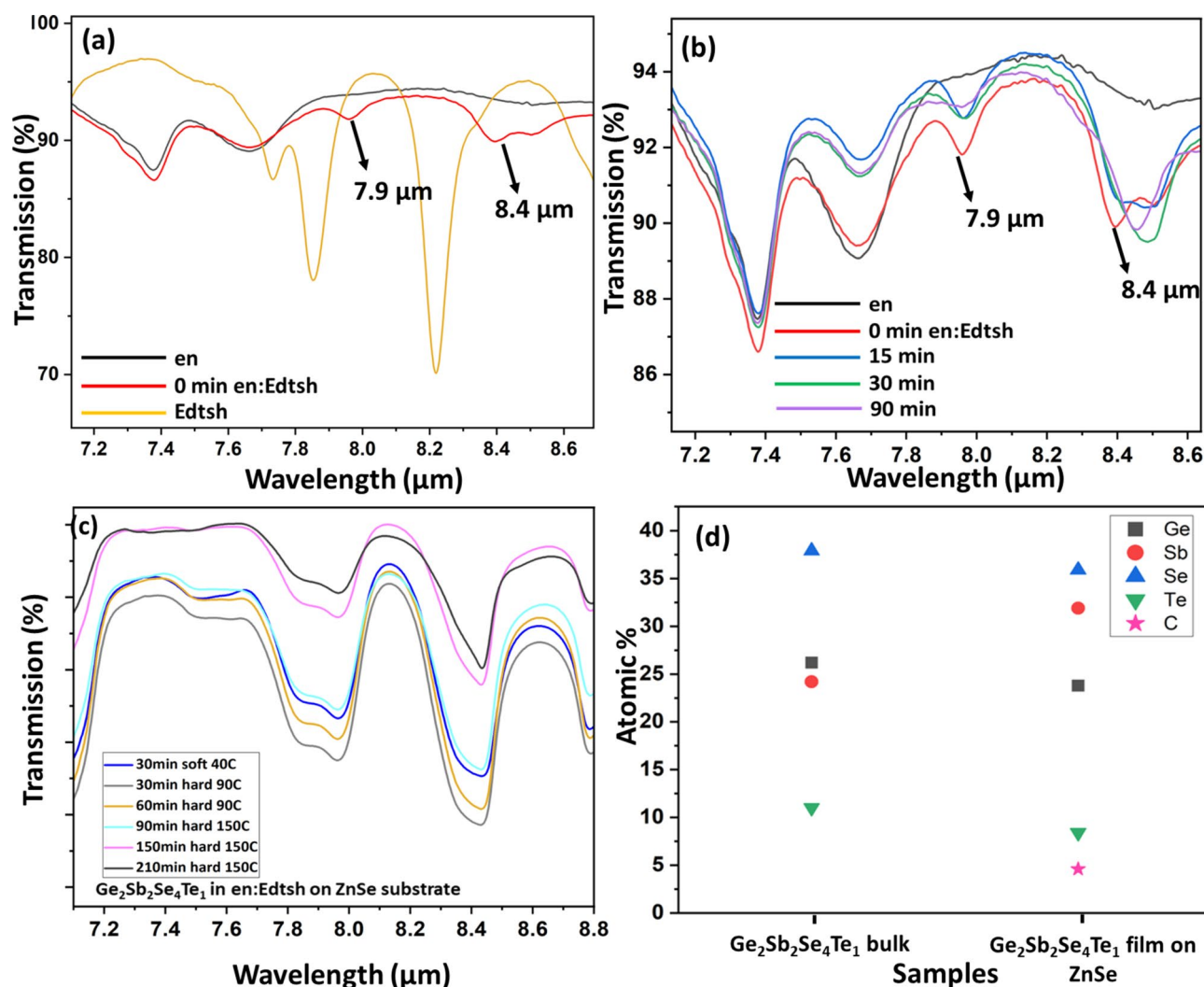


**Figure 7.** (a) Transmission spectra of the solvents, (b) Transmission spectra of the en:Edtsh solution with a volume-to-volume ratio of 10:1 when left standing at room temperature, (c) Transmission measurements of film deposited on ZnSe substrate as a function of bake protocol, (d) Comparison of the atomic % measured between a  $\text{Ge}_2\text{Sb}_2\text{Se}_4\text{Te}_1$  bulk alloy and a  $\text{Ge}_2\text{Sb}_2\text{Se}_4\text{Te}_1$  film deposited on ZnSe substrate after extended baking of the ZnSe substrate.

questions on the microscopic origin behind the thermodynamics and kinetics of PCMs but would also set a stage for their versatile incorporation into a wide variety of photonic devices.

### Experimental methods

The stoichiometries of parent powder and resulting films were extracted using the Noran System 7 EDS system with a silicon drift detector attached to the Zeiss ULTRA-55 FEG SEM. *In-situ* GIXRD measurement was performed using a PANalytical Empyrean system with a  $\text{Cu-K}_{\alpha 1}$  beam wavelength of 0.15418 nm, a beam voltage of 45 kV, a beam current of 40 mA, and a grazing incidence angle of  $< 0.1^\circ$  at multiple temperatures including RT, 150, 200, 300, and 400  $^\circ\text{C}$  under Ar atmosphere. At each elevated temperature, the coated film was held for 30 min, prior to the measurement. A ramping rate between each temperature was set to be 0.5  $^\circ\text{C}/\text{sec}$ . IR transparency of coated films was characterized up to a wavelength of  $\sim 20 \mu\text{m}$  using a ThermoFisher Nicolet iS5 FTIR Fourier-transform infrared spectrometer. The molecular structure of the glasses was analyzed using a Bruker Senterra micro-Raman spectrometer with an excitation laser wavelength of 785 nm and a power of 1 mW. Data were collected using a 50 s exposure and was accumulated over five scans in the range of 100 to 900  $\text{cm}^{-1}$ . A Mai Tai Ti:Sapphire laser with a center wavelength of 801 nm, a repetition frequency of 80 MHz, and a pulse width of  $< 100$  fs was used for direct laser writing of solution-derived films.

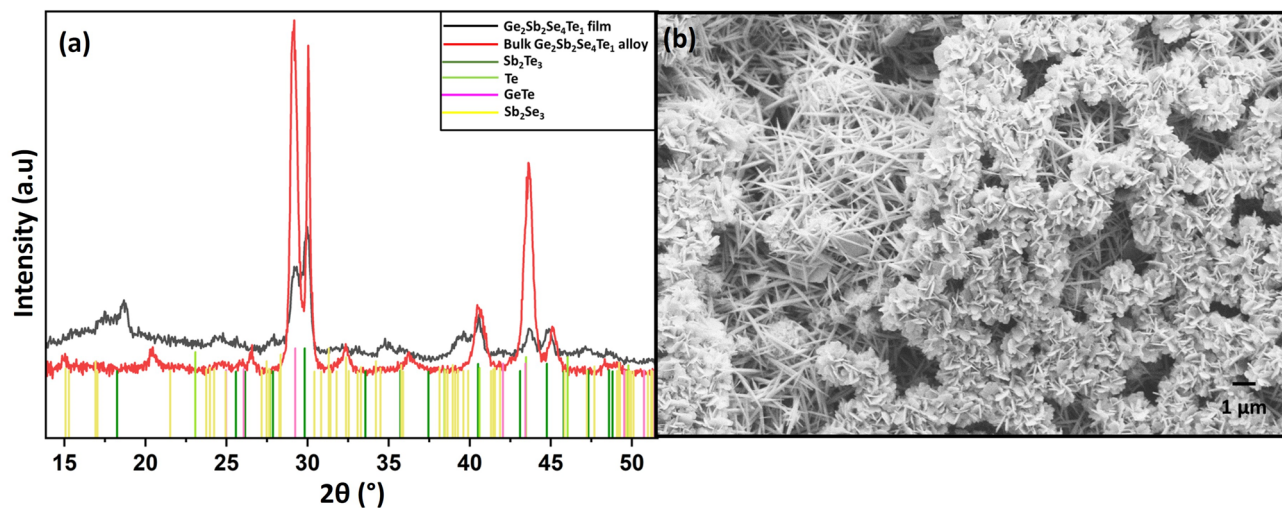


**Figure 8.** (a) XRD measurements of  $\text{Ge}_2\text{Sb}_2\text{Se}_4\text{Te}_1$  film and comparison of the peaks with bulk  $\text{Ge}_2\text{Sb}_2\text{Se}_4\text{Te}_1$  alloy, (b) SEM image of the en:Edtsh solution-deposited film baked at 350  $^\circ\text{C}$ , showing the needle shaped morphology of the  $\text{Ge}_2\text{Sb}_2\text{Se}_4\text{Te}_1$ .

### Data availability

The data that support the findings of this study are available from the corresponding authors upon reasonable request.

Received: 4 May 2024; Accepted: 30 July 2024

Published online: 05 August 2024

### References

- Wuttig, M., Bhaskaran, H. & Taubner, T. Phase-change materials for non-volatile photonic applications. *Nat. Photon.* **11**, 465 (2017).
- Friedrich, I., Weidenhof, V., Njoroge, W., Franz, P. & Wuttig, M. Structural transformations of  $\text{Ge}_2\text{Sb}_2\text{Te}_3$  films studied by electrical resistance measurements. *J. Appl. Phys.* **87**, 4130 (2000).
- Wuttig, M. & Yamada, N. Phase-change materials for rewriteable data storage. *Nat. Mater.* **6**, 824 (2007).
- Gholipour, B. The promise of phase-change materials. *Science* **366**, 186 (2019).
- Gholipour, B., Piccinotti, D., Karvounis, A., MacDonald, K. F. & Zheludev, N. I. Reconfigurable ultraviolet and high-energy visible dielectric metamaterials. *Nano Lett.* **19**, 1643 (2019).
- Michel, A.-K.U., Wuttig, M. & Taubner, T. Design parameters for phase-change materials for nanostructure resonance tuning. *Adv. Opt. Mater.* **5**, 1700261 (2017).
- Piccinotti, D. *et al.* Stoichiometric engineering of chalcogenide semiconductor alloys for nanophotonic applications. *Adv. Mater.* **31**, 1807083 (2019).
- Prabhathan, P. *et al.* A roadmap for phase change materials in photonics and beyond. *iScience* **26**, 107946 (2023).
- Abdollahramezani, S. *et al.* Electrical driven reprogrammable phase-change metasurface reaching 80% efficiency. *Nat. Commun.* **13**, 1696 (2022).
- Fang, Z. *et al.* Ultra-low-energy programmable non-volatile silicon photonics based on phase-change materials with graphene heater. *Nat. Nanotech.* **17**, 842 (2022).
- Wu, C. *et al.* Low-loss integrated photonic switch using subwavelength patterned phase change material. *ACS Photonics* **6**, 87 (2019).
- Fang, Z. *et al.* Non-volatile reconfigurable integrated photonics enabled by broadband low-loss phase change material. *Adv. Opt. Mater.* **9**, 2002049 (2021).
- Zhang, Y. *et al.* Broadband transparent optical phase change materials for high-performance nonvolatile photonics. *Nat. Commun.* **10**, 4279 (2019).
- Zhang, H., Wang, X. & Zhang, W. First-principles investigation of amorphous Ge-Sb-Se-Te optical phase-change materials. *Opt. Mater. Express* **12**, 2497 (2022).
- Zhang, Y. *et al.* Electrically reconfigurable nonvolatile metasurface using low-loss optical phase change material. *Nat. Nanotech.* **10**, 1038 (2021).
- Shalaginov, M. Y. *et al.* Reconfigurable all-dielectric metalens with diffraction-limited performance. *Nat. Commun.* **12**, 1225 (2021).
- Popescu, C.-C. *et al.* An open-source multi-functional testing platform for optical phase change materials. *Small Sci.* **3**, 2300098 (2023).
- Meng, J. *et al.* Electrical programmable multi-level non-volatile photonic random-access memory. *Light Sci. Appl.* **12**, 189 (2023).
- Schwartz, R. W. Chemical solution deposition of perovskite thin films. *Chem. Mater.* **9**, 2325 (1997).
- Zha, Y., Waldmann, M. & Arnold, C. B. A review on solution processing of chalcogenide glasses for optical components. *Opt. Mater. Express* **3**, 1259 (2013).
- Turnley, J. W. *et al.* Solution deposition for chalcogenide perovskites: A low-temperature route to  $\text{BaMS}_3$  materials (M = Ti, Zr, Hf). *J. Am. Chem. Soc.* **144**, 18234 (2022).
- Novak, S. *et al.* Direct electrospray printing of gradient refractive index chalcogenide glass films. *ACS Appl. Mater. Interfaces* **9**, 26990 (2017).
- Schenk, F. M. *et al.* Phase-change memory from molecular tellurides. *ACS Nano* **18**, 1063 (2024).
- Petit, L. *et al.* Compositional dependence of the nonlinear refractive index of new germanium-based chalcogenide glasses. *J. Solid State Chem.* **182**, 2756 (2009).

25. Waldmann, M., Musgraves, J. D., Richardson, K. & Arnold, C. B. Structural properties of solution processed  $\text{Ge}_{23}\text{Sb}_{7}\text{S}_{70}$  glass materials. *J. Mater. Chem.* **22**, 17848 (2012).
26. Webber, D. H., Buckley, J. J., Antunez, P. D. & Brutchey, R. L. Facile dissolution of selenium and tellurium in a thiol-amine solvent mixture under ambient conditions. *Chem. Sci.* **5**, 2498 (2014).
27. Boros, E. *et al.* On the dissolution of non-metallic solid elements (sulfur, selenium, tellurium and phosphorus) in ionic liquids. *Chem. Commun.* **46**, 716 (2010).
28. Lu, J., Xie, Y., Xu, F. & Zhu, L. Study of the dissolution behavior of selenium and tellurium in different solvents—a novel route to Se, Te tubular bulk single crystals. *J. Mater. Chem.* **12**, 2755 (2002).
29. Schwarz, C. M. *et al.* Structurally and morphologically engineered chalcogenide materials for optical and photonic devices. *J. Opt. Microsyst.* **1**, 013502 (2021).
30. Huang, S.-M. *et al.* The highly uniform photoresponsivity from visible to near IR light in  $\text{Sb}_2\text{Te}_3$  flakes. *Sensors* **21**, 1535 (2021).
31. Kim, S.-K., You, H.-K., Yun, K.-R., Kim, J.-H. & Seong, T.-Y. Fabrication of high-responsivity  $\text{Sb}_2\text{Se}_3$ -based photodetectors through selenization process. *Adv. Opt. Mater.* **11**, 2202625 (2023).
32. Li, J. *et al.* Performance limits of phase change integrated photonics. *IEEE J. Sel. Top. Quantum Electron.* **30**, 6100109 (2024).
33. Vitale, S. A. *et al.* Phase transformation and switching behavior of magnetron plasma sputtered  $\text{Ge}_2\text{Sb}_2\text{Se}_4\text{Te}$ . *Adv. Photon. Res.* **3**, 2200202 (2022).
34. Singh, M. P., Mandal, M., Sethupathi, K., Rao, M. R. & Nayak, P. K. Study of thermometry in two-dimensional  $\text{Sb}_2\text{Te}_3$  from temperature-dependent Raman spectroscopy. *Nanoscale Res. Lett.* **16**, 1 (2021).
35. Zybala, R. *et al.* Synthesis and characterization of antimony telluride for thermoelectric and optoelectronic applications. *Arch. Metall. Mater.* **62**, 1067 (2017).
36. Boschker, J. E. *et al.* Coincident-site lattice matching during van der Waals epitaxy. *Sci. Rep.* **5**, 18079 (2015).
37. Fleck, N. *et al.* Identifying Raman modes of  $\text{Sb}_2\text{Se}_3$  and their symmetries using angle-resolved polarized Raman spectra. *J. Mater. Chem. A* **8**, 8337 (2020).
38. Webber, D. H. & Brutchey, R. L. Alkahest for  $\text{V}_2\text{VI}_3$  chalcogenides: Dissolution for nine bulk semiconductors in a diamine-dithiol solvent mixture. *J. Am. Chem. Soc.* **135**, 15722 (2013).
39. Sharma, R. *et al.* Solution-based  $\text{Sb}_2\text{Se}_3$  thin films for microphotonics. *J. Opt. Microsyst.* **4**, 031203 (2024).
40. D. Wiedeman, R. Sharma, E. T. S. Bissell, P. Banerjee, C. M. Schwarz, B. Mills, D. Callahan, J. Hu, and K. A. Richardson. Solution based processing of GSST (2241) for optical phase change materials. *Submitted*.

## Acknowledgments

This work was funded by Defense Advanced Research Projects Agency through the Defense Sciences Office's EXTREME Optics and Imaging (EXTREME) program under award number HR00111720029 as well as National Science Foundation through multiple programs. Specifically, the Addressing Systems Challenges through Engineering Teams (ASCENT) program under award number #2132929 and the Combinatorial Solution Processing of Optical Phase Change Materials under award number #2225967. The views, opinions, and/or findings expressed are those of the authors and should not be interpreted as representing the official views or policies of the Department of Defense. R.S. acknowledge the partial support of the University of Central Florida's Pre-eminent Post-doctoral Scholar Program (P3).

## Author contributions

M.K. project administration, investigation, resource, analysis, and wrote the manuscript. R.S. resource, analysis, and wrote the manuscript. C.B. resources. D.W. resources. Q.A. resources. P.E.L. resources. G.B.J.S.T. resources. Y.Z. resources. M.Y.S. resources. C.-C.P. resources. B.M.T. resources. C.R.-B. resources. C.M.S. resources. A.M.A. resources. T.G. resources. J.H. project administration, investigation, and resources. K.A.R. project administration, investigation, and resources. All the authors reviewed the manuscript.

## Competing interests

The authors declare no competing interests.

## Additional information

**Correspondence** and requests for materials should be addressed to M.K.

**Reprints and permissions information** is available at [www.nature.com/reprints](http://www.nature.com/reprints).

**Publisher's note** Springer Nature remains neutral with regard to jurisdictional claims in published maps and institutional affiliations.

**Open Access** This article is licensed under a Creative Commons Attribution-NonCommercial-NoDerivatives 4.0 International License, which permits any non-commercial use, sharing, distribution and reproduction in any medium or format, as long as you give appropriate credit to the original author(s) and the source, provide a link to the Creative Commons licence, and indicate if you modified the licensed material. You do not have permission under this licence to share adapted material derived from this article or parts of it. The images or other third party material in this article are included in the article's Creative Commons licence, unless indicated otherwise in a credit line to the material. If material is not included in the article's Creative Commons licence and your intended use is not permitted by statutory regulation or exceeds the permitted use, you will need to obtain permission directly from the copyright holder. To view a copy of this licence, visit <http://creativecommons.org/licenses/by-nc-nd/4.0/>.

© The Author(s) 2024